Experimental quality assessment of thermoplastic composite corner regions manufactured using laser-assisted tape placement

Peeters, Daniël; Jones, David; O'Higgins, Ronan; Weaver, Paul M.

Important note
To cite this publication, please use the final published version (if applicable).
Please check the document version above.

COMPOSITE
STRUCTURES

EDITOR: A. J. M. FERREIRA

Check for
updates

Experimental quality assessment of thermoplastic composite corner regions manufactured using laser-assisted tape placement

Daniël Peeters [a,b], David Jones [a], Ronan O'Higgins [a,*], Paul M. Weaver [a]

[a] *School of Engineering and Bernal Institute, University of Limerick, Ireland*
[b] *Faculty of Aerospace Engineering, Delft University of Technology, Kluyverweg 1, Delft, 2629HS, The Netherlands*

ARTICLE INFO

ABSTRACT

Over the past 25 years, interest in thermoplastic composites in aircraft has steadily increased. Combining winding and laser-assisted tape placement is a promising method to manufacture thermoplastic structures using in-situ consolidation, as shown recently by manufacturing a variable stiffness, unitized, integrated-stiffener thermoplastic wingbox at the University of Limerick. The corner regions are a critical point of the structure and require in-depth characterization studies, for example by unfolding L-shaped samples in a 4-point bend test. In this work, samples with radii varying from 2 to 10 mm were manufactured and tested. Two manufacturing parameters were varied: the rotational speed and acceleration of the tool. Test data show that decreasing the radius increases the corner strength, but an optimum radius exists to withstand a maximum unfolding force/moment. In addition, the slowest deposition rate with least acceleration of the head used during manufacturing lead to the highest corner strength for the same radius.

1. Introduction

Over the past decades, interest in using thermoplastic composites (TPC) in commercial and military aircraft has grown. Starting with one of their first applications with the US military's F-22 fighter jet landing-gear and weapons-bay doors [1], applications now include, among many others, the fixed wing leading edge on the Airbus A380 [2]. TPCs are of interest due to their potential for fast forming and weldability, their superior toughness and their excellent fire/smoke/toxicity properties compared with thermoset composites. Furthermore, the potential of these materials to manufacture large aerospace structures in a cost effective manner using in-situ consolidation is appealing and has been a topic of research for many years [3–5].

A couple of years ago, an in-situ consolidated, variable stiffness, unitized, integrated-stiffener thermoplastic wingbox demonstrator was built and successfully tested at the University of Limerick [6]. An advantage of a unitized structure is the intrinsically lower assembly costs: the wingbox is one single part, in contrast to a conventionally constructed wingbox, which uses angle sections to connect skins to webs. This unitizing also has a disadvantage: unlike traditional metallic structures, no L-brackets are reinforcing the corners. Hence, all section forces have to be transmitted through the corners by the composite material, without any extra reinforcement. Stress analysis of the wingbox shows that the highest stress occurs in the corners, as shown in Fig. 1, where the normal stress in the fibre direction is shown.

Both the wingbox and the stiffeners were made using winding in combination with laser-assisted automated tape placement (LATP). Detailed characterization of coupon specimens harvested from the wingbox was however limited, as only one demonstrator was produced. Another critical part, namely the connection between skin and stiffener, was characterized in more detail: the bond strength was found to be satisfactory (46 MPa) [7]. However, the tests determining the strength of the corners were inconclusive [8]. A typical outcome of the 4-point bend test on an L-shaped specimen is shown in Fig. 2. The test was inconclusive because the test standard could not be adhered to: the legs of the test piece were too short because the stiffener was too small, the lay-up was not according to the standard, and the initial angle was not 90° but larger. The reason for failure could not be determined: it was attributed to either the 3-dimensional stress introduced into the tested part because of the close roller spacing, the radius of the samples being too small, or the used manufacturing parameters. In the current study, L-shaped test samples with dimensions that respect the guidelines of the ASTM test standard [9] were manufactured to assess the performance of corner structures produced by the LATP winding process.

When using thermoset material, producing a perfect 90° L-shaped sample is challenging due to spring-in during cooling [10]. Another manufacturing defect that can occur is wrinkling. This defect arises from the length difference between the inner and outer radii of a

---

* Corresponding author.
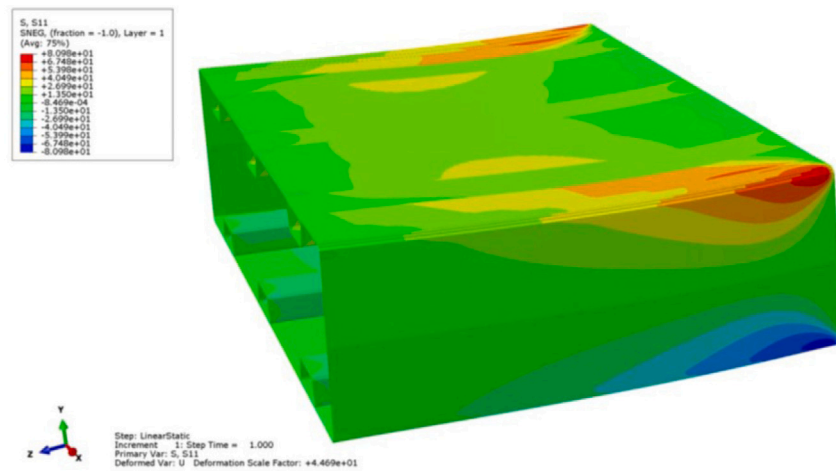*E-mail address:* ronan.ohiggins@ul.ie (R. O'Higgins).
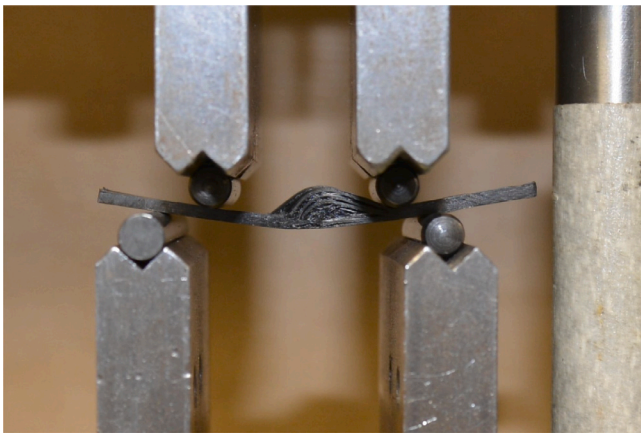
Fig. 1. σ_{11} for the wingbox.

Fig. 2. Example of 4-point bend test outcome.

corner [11]. When wrinkling occurs, the amount of spring-in is reduced: the inherently lower effective stiffness of the wrinkled layer leads to a lower resulting force generated by the cooling down after curing, reducing the amount of spring-in. Experimentally, the number of wrinkles that occurred was increased by bending the complete stack, rather than by forming each ply individually while laying down the material [12].

Other manufacturing techniques to manufacture L-shaped samples include pultrusion, braiding, compression moulding, and stamp forming. Pultrusion involves pulling fibres through a die to achieve the desired profile. Using this technique, the spring-in angle was found to be varying with the distance from the die exit [13,14]. A combination of braiding and pultrusion can also be used, but the achievable lay-ups are restricted: no uni-directional part can be achieved, for example. The resulting structure combining braiding and pultrusion has been found to be well consolidated [15]. Also stamp forming can be used [16], which recently was shown to be viable after automated lay-up of a blank to rapidly obtain curved thermoplastic parts [17]. A more general overview can be found in Ismet et al. [14]

The current study focuses on assessing the structural performance of LATP wound corners with in-situ consolidation, hence without any post-processing step after lay-up. This work builds up from the work presented during the 18th European Conference on Composite Materials [18]. Samples with dimensions according to ASTM Standard D6415 [9] were produced by manufacturing a box and harvesting L-shaped test samples from it. Both the geometry and manufacturing parameters were investigated by varying the radius of the sample

and rotational speed and acceleration during manufacturing. Four-point bend testing was performed to assess the performance of the corner specimens. The results of this study were compared with results from similar studies for composites produced by other manufacturing methods.

2. Manufacturing

2.1. Laser assisted fibre placement system and set-up

L-section test specimens were harvested from LATP wound square box sections. Two different tools were used. The first tool has a corner radius of 10 mm on each corner. The second tool is more versatile, with a different radius on each corner: 2, 4, 6, and 8 mm are all used. These geometries allow to study the influence of the radius of the tool and different manufacturing parameters.

The rotational speed and acceleration at the corner were varied during the manufacturing trials. The LATP system used was provided by AFPT GmbH and is installed at the University of Limerick. During manufacture, the laser power is controlled using a temperature-feedback loop: the temperature at the nip point (i.e., the point where the roller presses the incoming tape onto the substrate) is aimed to be 400 °C, and the power is constantly adapted to stay as close as possible to this temperature. The laser angle relative to the substrate was adapted before each layer such that the focus of the laser was close to the nip point. The laser spot size was 20 mm wide in the tape direction and 40 mm along the length of the tape. The material used was provided by Toho Tenax: TPUD PEEK-IMS65. The tape material was slit to a width of 6.35 mm, with a fibre volume fraction of 60%. A single tape was laid down at a time. The nominal thickness of a layer was 0.18 mm. The pneumatic pressure on the compaction cylinder was set to 2.5 bar, with a spring allowing to take up small thickness variations without changing the pressure. The roller used was a conformable silicone roller, provided by AFPT.

2.2. Tooling

The constant 10 mm-radius tool consists of steel sides as shown in Fig. 3. The corners are made out of solid circular aluminium bars. The original intend of this tool was to produce four plates by winding, and scrapping the corners, but will now be used to manufacture the corners. The take the manufactured part of, the tool is made to collapse inwards, by removed the aluminium corner bars.

Since this work focuses on producing corner specimens, removal of the tool without damaging the corners is important. This undamaged removal proved challenging since the corner supports were forcefully
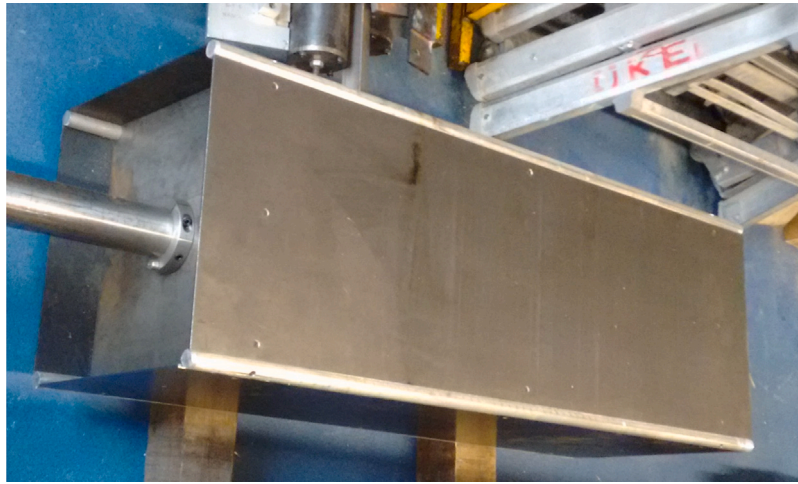
Fig. 3. Tool with a 10 mm radius.

removed, which could potentially damage the corner specimens. Alternatively one steel surface plate was removed, followed by cutting the box along this surface. Both tool removal methods were used, with a significant effect on testing results, which are discussed in Section 4.

Another tool was designed to manufacture corner specimens with different radii in one go, without the need to always change the tool. This tool consists of four aluminium 100×100 mm box sections with a wall thickness of 5 mm. Radii of up to 8 mm can be machined at the corner. By using a different radius on each of the four corners, specimens with four different radii can be produced in one go. Radii of 2, 4, 6, and 8 mm were chosen in the current work: 2 mm was considered to be the lower limit from a manufacturing point of view, while 8 mm was the constraint based on the wall thickness of the box sections. However, the radius of each corner can easily be changed as the box sections are interchangeable and can have different radii on different sides. To be able to remove the specimens undamaged, a 2 mm thick aluminium spacers are placed in between the box sections to make the tool collapsible. After manufacture, the spacers are taken out, which gives sufficient leeway to gently slide the boxes out without damaging the specimens. To ensure the spacers can be taken out, the radius arc length is only made over 500 mm, leaving 250 mm on either side. To stiffen the tool during manufacture, steel end-plates are used which interface tightly with the aluminium box sections. The tool assembly is shown in Fig. 4. On the top left an 8 mm radius is shown, on the top right a 2 mm radius is created. The 2 mm gap is clearly shown at the back of the tool, while the spacer is shown in the front of the picture.
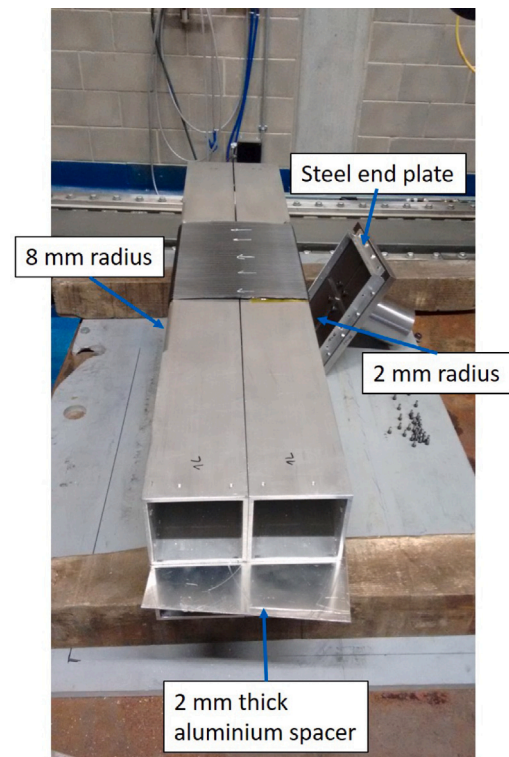
2.3. Influence of manufacturing parameters

The key manufacturing parameters examined are the rotational speed of the tool and acceleration around the corners. As this study complements previous work [6], the linear speed over the straight parts remains unchanged at 3 m/min. During rotation the head of the robot has to accurately move over a significant distance which limits the maximum attainable speed: the tape is always placed on the top part of the tool, hence the tool is rotated after each side has been placed. The tool rotational speed and acceleration were $200°/s$ and $1000°/s^2$ respectively. Due to the moment of inertia of the tool, and the torque provided by the motors, no higher rotational speed or acceleration were tested.

To assess the effect of processing parameters on the corner strength, specimens were manufactured with varying rotational speed, rotational acceleration and thickness according to Table 1. In this table we refer to boxes since physically we manufacture a box that is afterwards cut into L-shaped specimens. Two rounds of manufacturing were undertaken

Fig. 4. Tool with a 2, 4, 6, and 8 mm radius.

using the 10 mm radius tool (box 1 to 4 in round one; box 5 to 7 in a second round). Box 1 is used to assess if thinner specimens can be used, while box 2 is made according to the same manufacturing parameters as used in previous work [8], and thus is regarded as the reference case in the current work. Box 1 to 4 were demoulded by forcefully removing the aluminium bars from the tool, which damaged two corners of box 2, reducing the amount of usable samples to four. Box 5 to 7 were demoulded by removing one of the steel plates and cutting one of the edges in the middle, which the authors believe leads to less (or no) damage in the tested samples.

To perform the corner strength tests according to ASTM 6415, L-shaped specimens were cut from the box coupons and sanded down to a smooth finish. All sample dimensions satisfied the standard requirements [9] as shown in Fig. 6. No visual delamination was observed on

Table 1
Overview of the manufacturing parameters and thicknesses.

Box number [−]	Rotational speed [°/s]	Rotational acceleration [°/s²]	Radius [mm]	Average thickness 1 (std. dev.) [mm]	Average thickness 2 (std. dev.) [mm]	Average thickness 3 (std. dev.) [mm]
1	200	1000	10	1.070 (0.031)	1.087 (0.013)	1.075 (0.030)
2	200	1000	10	2.378 (0.053)	2.202 (0.032)	2.332 (0.063)
3	150	750	10	2.216 (0.038)	2.189 (0.039)	2.237 (0.054)
4	200	750	10	2.152 (0.042)	2.106 (0.024)	2.132 (0.054)
5	200	1000	10	2.360 (0.056)	2.461 (0.045)	2.340 (0.040)
6	150	750	10	2.300 (0.028)	2.408 (0.045)	2.304 (0.034)
7	100	500	10	2.428 (0.025)	2.508 (0.032)	2.404 (0.021)

Table 2
Overview of the manufacturing parameters and thicknesses for the different radii.

Rotational speed [°/s]	Rotational acceleration [°/s²]	Radius [mm]	Average thickness 1 (std. dev.) [mm]	Average thickness 2 (std. dev.) [mm]	Average thickness 3 (std. dev.) [mm]
200	1000	2	2.322 (0.030)	2.384 (0.026)	2.333 (0.030)
200	1000	4	2.314 (0.023)	2.348 (0.021)	2.310 (0.023)
200	1000	6	2.326 (0.015)	2.356 (0.021)	2.308 (0.021)
200	1000	8	2.344 (0.015)	2.370 (0.020)	2.345 (0.024)
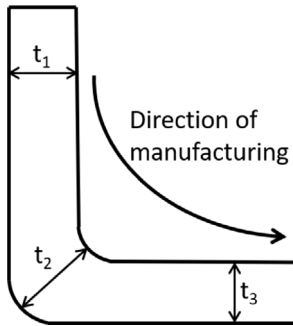
Fig. 5. Numbering of the points at which the thickness is measured.

any of the samples, however, the samples harvested from boxes 5 to 7 are believed to have less internal damage due to the removal method. No detailed microscopy has been performed to confirm these finding since the difference in results was only apparent after performing the tests.

Before testing, the thickness of the different legs were measured using a micrometer with flat measuring tips. In Table 1, thickness 1 denotes the thickness in the leg before the corner, thickness 2 is the thickness in the corner, and thickness 3 denotes the thickness in the leg after the corner, as shown in Fig. 5. The general trend in this table for the first 4 boxes is that the corners themselves are thinner than the legs before and after. Only box 1 shows a different trend, however, this difference is relatively small and could be due to the accuracy of the measurements. The largest thickness was observed in box 2. For box 5 to 7, where the same manufacturing parameters were used as for box 1 to 4, a different trend was observed: the corner is slightly thicker. The thickness of the straight edges are similar, indicating the consistency of the manufacturing process for different runs.

2.4. Influence of radius

Using the new tool with the different radii, the influence of the radius on the corner strength was assessed. In total, four different radii were tested. The manufacturing parameters were set to the reference values, that were also used in a previous work [8]. Considering the thickness of the legs, from Table 2, it is observed that they are all almost identical to each other. Hence, the radius of the corners has no influence on the thickness of the corners.

3. Tests

To assess the corner strength, 4-point bending tests were executed according to ASTM Standard D6415 [9] A schematic of the structure is shown in Fig. 6(a). Box 1.1 deviated from the standard because it is only 1.1 mm thick. The other boxes complied better, but since we want to investigate the effect of the radius, the prescribed radius of 6.4 mm is not adhered to. Other than these two changes, the test specimens comply with the ASTM standard.

The methodology described in the ASTM standard is used to calculate the curved beam strength (CBS) [9]:

$$CBS = \frac{M}{w} = \left(\frac{F}{2 \cdot w \cdot cos(\phi)} \right) \cdot \left(\frac{d_x}{cos(\phi)} + (D + t) \cdot tan(\phi) \right) \quad (1)$$

where M denotes the moment, w the width of the specimen, F the total force, ϕ the angle, D the diameter of the cylindrical loading bars, t the thickness of the sample and d_x the distance in x-direction between the upper and lower bar. These dimensions are shown schematically in Fig. 6(b). The angle ϕ changes during the test, and can at any moment during the test be calculated using

$$\phi = Arcsin \left(\frac{-d_x \cdot (D + t) + d_y \cdot \sqrt{d_x^2 + d_y^2 - D^2 - 2 \cdot D \cdot t}}{d_x^2 + d_y^2} \right) \quad (2)$$

where d_y denotes the distance in the y-direction between the inner and outer roller, calculated using

$$d_y = d_x \cdot tan(\phi_0) + \frac{D + t}{cos(\phi_0)} - \Delta \quad (3)$$

where the subscript 0 denotes the initial angle (i.e., at the start of the test), and Δ denotes the displacement in y-direction of the rollers.

Next to the CBS, we can also calculate the radial stress in the corner. The radial stress in a curved beam segment can be calculated using the method originally proposed by Lekhnitskii [19]. By calculating the radial stress, the result is no longer dependent on the sample radius, and thus can be compared to each other. The stress in the radial direction can be calculated using [19]

$$\sigma_r = -\frac{CBS}{r_o^2 \cdot g} \cdot \left(1 - \frac{1 - \rho^{\kappa+1}}{1 - \rho^{2\kappa}} \left(\frac{r_m}{r_o} \right)^{\kappa-1} - \frac{1 - \rho^{\kappa-1}}{1 - \rho^{2\kappa}} \rho^{\kappa+1} \left(\frac{r_o}{r_m} \right)^{\kappa+1} \right) \quad (4)$$

where r_o denotes the outer radius of the test specimen. The other terms are defined as

$$g = \frac{1 - \rho^2}{2} - \frac{\kappa}{\kappa + 1} \cdot \frac{\left(1 - \rho^{\kappa+1}\right)^2}{1 - \rho^{2\kappa}} + \frac{\kappa\rho^2}{\kappa - 1} \cdot \frac{\left(1 - \rho^{\kappa+1}\right)^2}{1 - \rho^{2\kappa}} \quad (5)$$
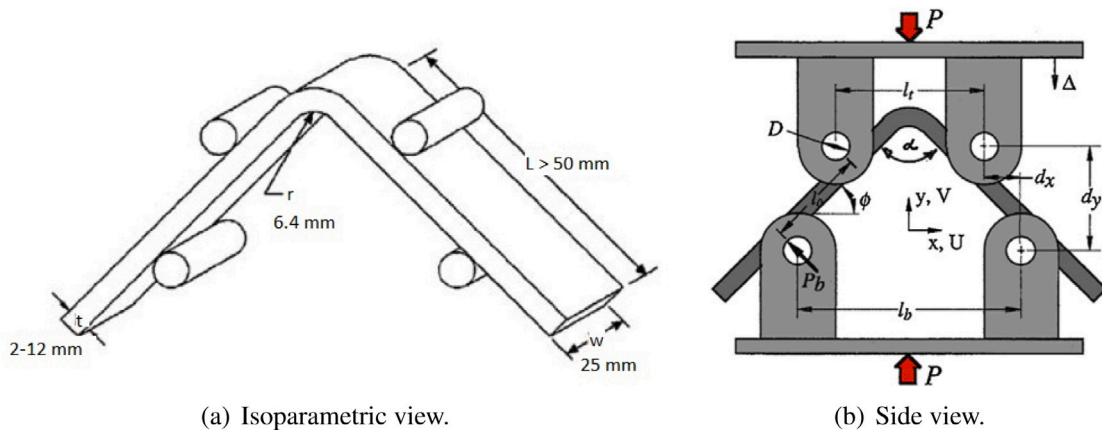
(a) Isoparametric view.

(b) Side view.

Fig. 6. Schematic view of the 4-point bend test according to ASTM D 6415.

$$\kappa = \sqrt{\frac{E_\theta}{E_r}} \tag{6}$$

$$\rho = \frac{r_i}{r_o} \tag{7}$$

$$r_m = \left(\frac{\left(1 - \rho^{\kappa-1}\right) \cdot (\kappa+1) \cdot \left(\rho r_o\right)^{\kappa+1}}{\left(1 - \rho^{\kappa-1}\right)(\kappa-1) r_o^{-(\kappa-1)}} \right)^{\frac{1}{2\kappa}} \tag{8}$$

where E_θ is the E_{11} modulus and E_r can be assumed to be E_{22}. For the material used in this work $E_{11} = 135$ GPa and $E_{22} = 7.54$ GPa.

While testing boxes 1 to 4, delaminations were observed to initially occur in the leg that was manufactured before the corner. The delaminations occurred suddenly: a cracking sounds was heard, immediately followed by a significant drop in load. This behaviour suggests that the bond achieved in the corner was as good or even better than that achieved in the legs.

3.1. Different manufacturing parameters

The average radial stress at maximum load and corner beam strength for each of the four boxes is shown in Figs. 9 and 10 respectively. The exact numerical values can be found in Table A.3. For boxes 2 and 3 only four samples were tested due to manufacturing and testing issues respectively. For boxes 1 and 4, the testing was performed on 8 samples. The standard deviations observed are relatively small for box 1, 2, and 4, only for box 3 the tests show considerable scatter.

The results of boxes 1 to 4 indicate that the benchmark (box 2) gives the largest radial stress. Even though the same manufacturing parameters were used for box 1, the radial strength is more than 10% lower. However, this specimen was half the thickness recommended by the test standard and the failure mechanism is different compared to the other specimens, agreeing with the theoretical prediction of Thurnherr et al. [20]. Reducing the rotational acceleration and speed does not lead to a higher corner strength, on the contrary: the maximum radial stress is reduced by 8% when the acceleration is reduced to $750°/s^2$, and by 12% when the speed is reduced to $150°/s$ and acceleration to $750°/s^2$. However, due to the limited number of samples tested, as well as the possibility that removing the boxes from the mould may have induced defects in the specimens, these findings were checked by manufacturing another three boxes and de-moulding them using the alternative method described in Section 2.

The results from boxes 5 to 7 contradicted the previous results. Slowing down the speed and acceleration for these boxes produced specimens with a higher corner strength. The difference between boxes with the same manufacturing settings (box 2 and 5, and box 3 and 6) was found to be significant. However, when investigating the load–displacement diagrams, shown in Figs. 7 and 8, it appears that all samples exhibit a similar stiffness, but the samples from box 5 and 6 break at a higher load and greater displacement. The increased displacement leads to a lower radial strength, but the corner beam strength increases. The authors believe that the force that is consistently higher for box 5 and 6 is the result of less defects (e.g., micro-cracks) due to the more gentle demoulding technique. Unfortunately all samples were tested so no additional checks (e.g., optical microscopy or C-scan) could be performed to verify this hypothesis. Hence, it is believed that the lower speed and acceleration leads to corners with a higher strength.

3.2. Different radii

The results for the different radii are provided in Figs. 13 and 14. The exact numerical values can be found in Table A.4. Each result presented is the average from eight test specimens. For a number of tests, initial cracks were observed to form on one side of the specimen, but not delaminating all through the width, resulting in significant twisting that induced an increase in load after the crack formation. An example of this phenomenon is shown in Fig. 11. As a reference, the load–displacement graph for all samples with a radius of 2 mm is shown in Fig. 12. The force and displacement readings to compute the values in Figs. 13 and 14 were taken when the first crack appears, which is evidenced by a (small) drop in load or a distinct change in slope of the load–displacement graph. This choice was made since the assumptions used to calculate the stress are no longer satisfied once the specimen starts to twist. The standard deviation for all cases is well below 10% showing good consistency between tests. In addition, the loading curves, shown in Fig. 12, show consistency across the specimens, which was observed for all tested radii.

The results in Figs. 13 and 14 show that for the different radii the maximum displacement lies within 7% of each other while the force differs by up to 24%. The force at delamination and CBS is clearly largest for a 6 mm radius. The radius has a significant influence on the radial stress: even though the force and CBS are significantly smaller (24%) for a 2 mm radius than for a 6 mm radius, the radial strength is more than 75% larger. Hence, in order to compare the different radii, CBS should be used, not the radial strength.

An explanation for the better performance of the 6 mm radius is hard to determine. When using a smaller radius, the distance travelled while rotating the tool is apparently too short to achieve a good bond: the length to accelerate and decelerate is too short. For the larger radii, better bond performance is expected based on the acceleration and deceleration in the corner. However, when approaching a corner, the laying speed is decreased. The larger the radius, the further away from the straight-angle cross-section this decrease happens. This slowing down may decrease the bond strength further in the legs of the specimen, leading to delamination at a lower load. Hence, the 6 mm radius seems to be a good compromise between the arc-length of the corner and the decreasing speed before the corner.
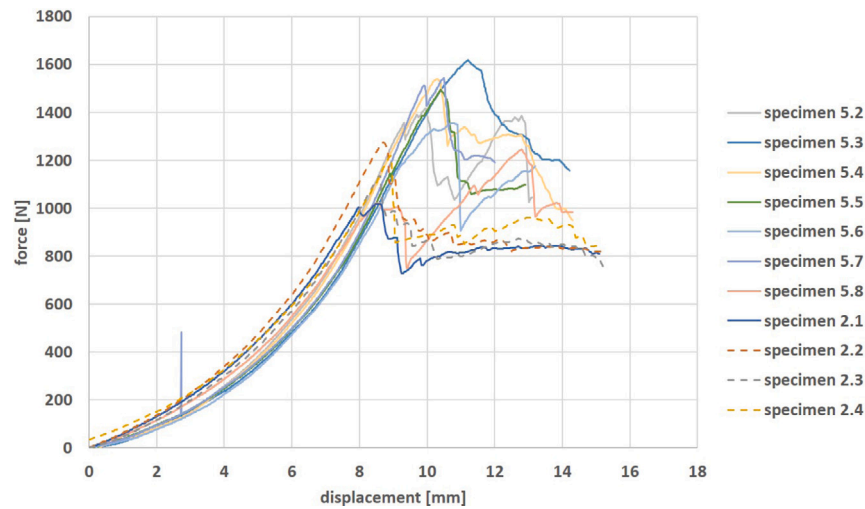
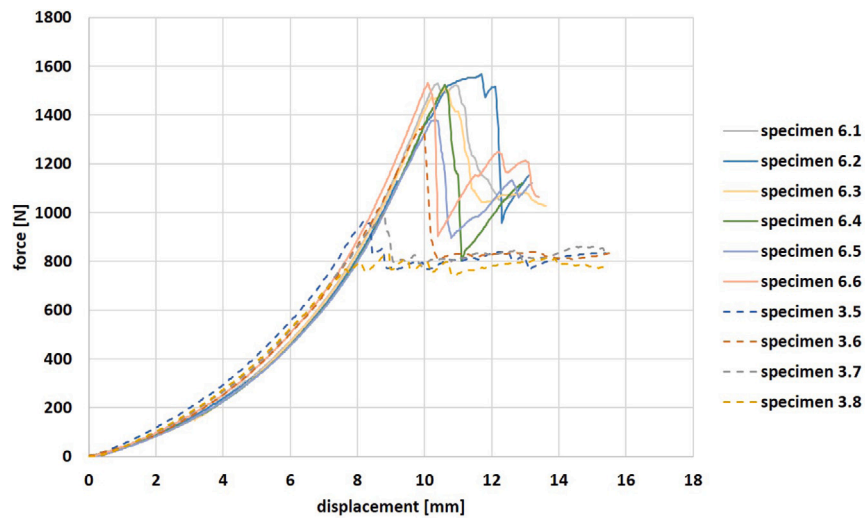**Fig. 7.** Force–displacement graph for specimens taken from box 2 and 5.

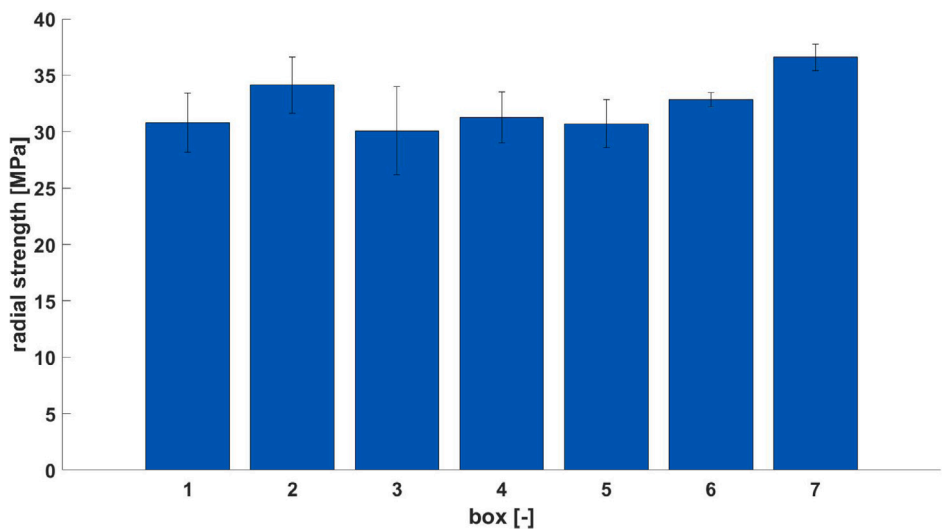**Fig. 8.** Force–displacement graph for specimens taken from box 3 and 6.

Fig. 9. Radial strength for boxes 1–7 (errors bars indicate the standard deviation).
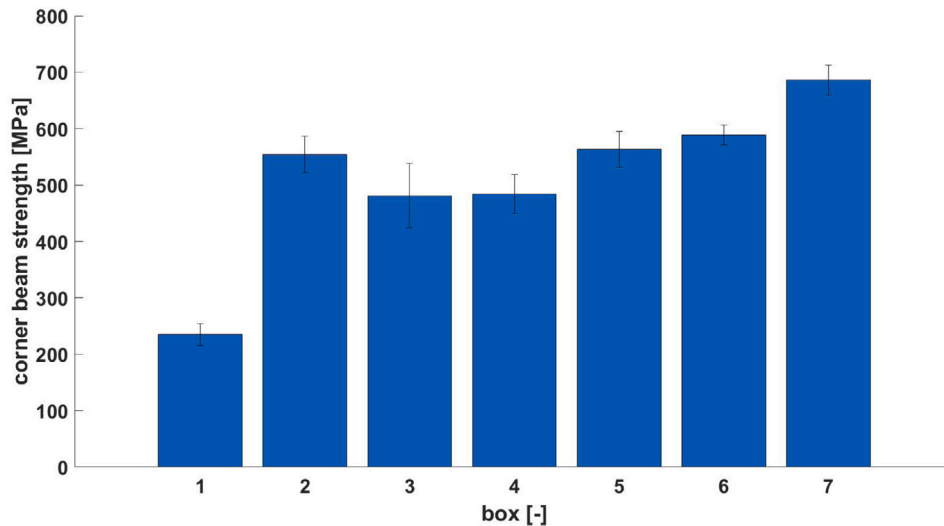
Fig. 10. Corner beam strength for boxes 1–7 (errors bars indicate the standard deviation).
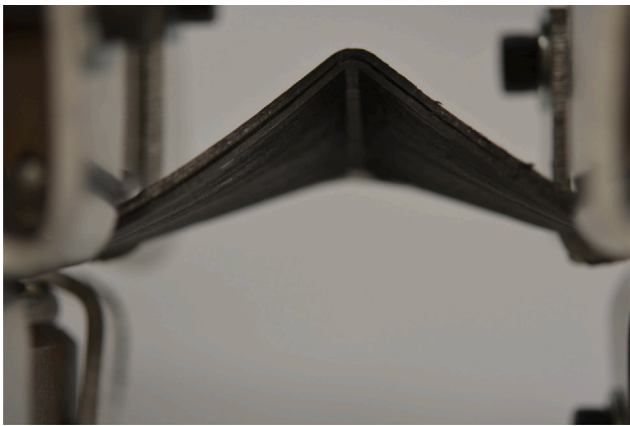

Fig. 11. Radius 2 mm, specimen 8 at the end of the test.

4. Discussion

To compare to results in literature, we need a metric that is independent of the thickness, since the thickness of the results in literature is often varying. The metric that is best suitable for this purpose is the radial strength [21,22]. Only one article was found where a clear difference in radial strength for samples with different thickness was measured [23], however no specific reason is given for this. Comparing the current results to literature is not straightforward since no results for the same material, or any other CFRP thermoplastic with continuous fibres for that matter, were found after a literature search. Hence, we will compare to samples made using thermoplastic with short fibres, and thermoset material.

Using a thermoplastic matrix and short carbon fibres [24], a radial strength of 21 MPa was measured for a thickness of 2 mm, independent of the radius being 3 or 5 mm. When increasing the radius further, the radial strength decreased to 12 MPa. The radial strength decreasing with an increasing was also observed in our measurements. The magnitude of the stress on the other hand does differ: the radial stress achieved in the current work is more than quadrupled compared to the short fibre samples in literature. This difference is most likely due to the uni-directional lay-up with continuous fibres used in the current work.

For thermoset composite materials, the radial strength data presented in literature varies between of 27 and 40 MPa [21,22,25]. With the radius equal to the thickness, a radial strength of 36–40 MPa was measured for a range of thicknesses (4, 8, and 12 mm), independent of the lay-up [21]. Another study found a radial strength of around 30 MPa for 3 and 6 mm thick specimens with a radius of either 3 or 6 mm [22]. In other work, Redman et al. [25] measured 27–28 MPa as radial strength for a 3 mm thick specimen. The only study that finds a significantly lower radial strength was performed on thick laminates: 20, 40 and 60 plies (respectively 3.8, 7.6 and 11.4 mm thick), with a radius to thickness ratio of 0.8, 1 and 1.5 [23]. The radial strength was 7–8 MPa for the thinnest laminate and only 4–5 MPa for the thickest laminate. Based on the current results, the difference could be attributed, at least in part, to the larger radius compared to the other works.

Comparing the current results for box 1 to 7 (i.e., a constant 10 mm radius) to the results in the literature for thermoset material, one can conclude that the radial strength is found to be comparable: the current results vary from 30 to 36 MPa, which is comparable to the 27 to 40 MPa range in literature. However, it was shown that the 10 mm radius used in these boxes did not achieve the highest radial strength. The radii used in the literature are often smaller, which is shown in the current work to lead to a significant increase (almost tripled when a radius of 2 mm was used) in radial strength.

While radial strength increased with decreasing radius, the opposite trend was observed for CBS and measured maximum load. The ratio of the radius to laminate thickness better explains the influence of corner radius on structural performance: since the thickness is constant this ratio changes significantly. The 6 mm radius is found to have the highest CBS, which is probably because it is a good compromise between the distance travelled in the corner (which will lead to an increase in CBS with an increasing radius) and the decrease in speed before the corner (leading to the laser having to adapt and going outside the optimal processing window). However, regardless of the radius (and radius-to-thickness ratio) the results do show that corners of good quality can be manufactured: the load and moment that they can carry is significant even for the smallest radius tested.

When considering the influence of the manufacturing parameters, it is observed that a lower speed and acceleration leads to corners of higher strength. One of the reasons is that due to the slower speed, the roller presses down on the tape longer, and the tape can cool down to a lower temperature while pressure is applied. Another reason could be the temperature feedback used to control the laser: if the speed and acceleration are lower, the distance travelled at temperatures that are outside the ideal processing window is shorter, and thus the quality of the laminate is better. To eliminate this effect, one could program the
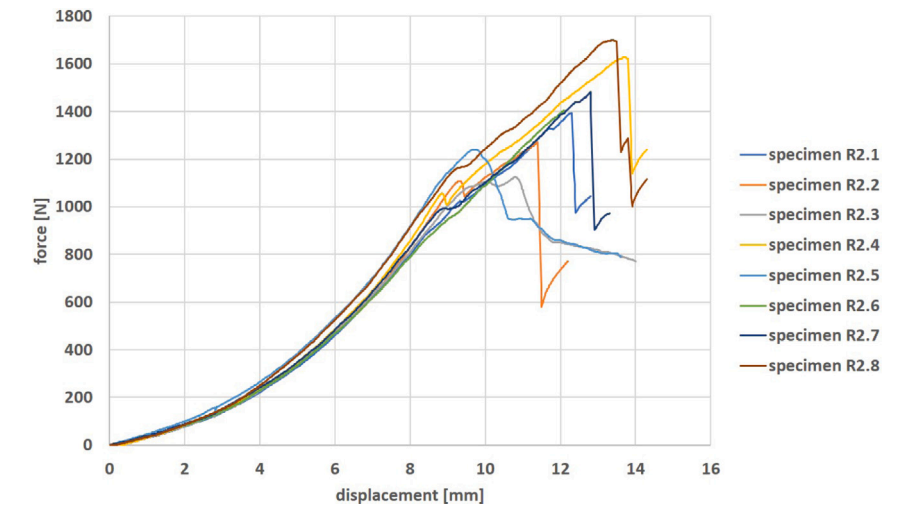
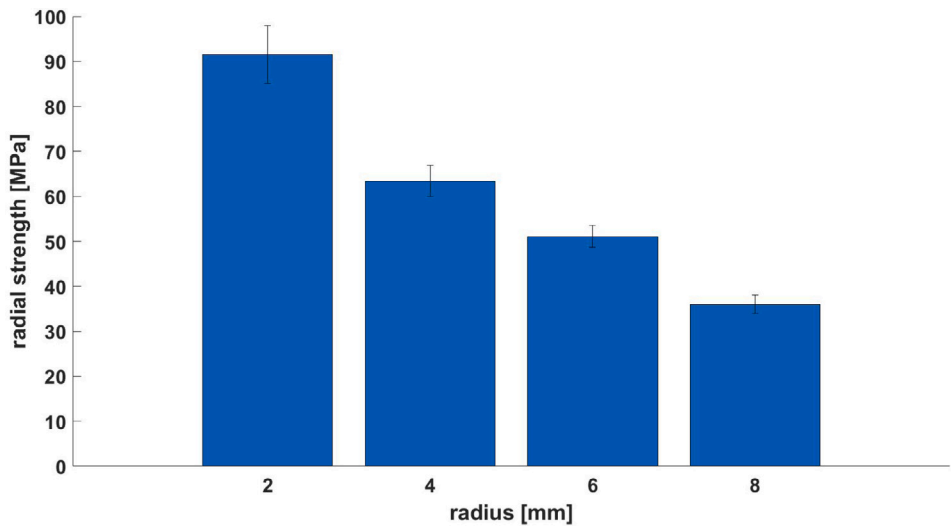**Fig. 12.** Force–displacement graph for specimens with a radius of 2 mm.

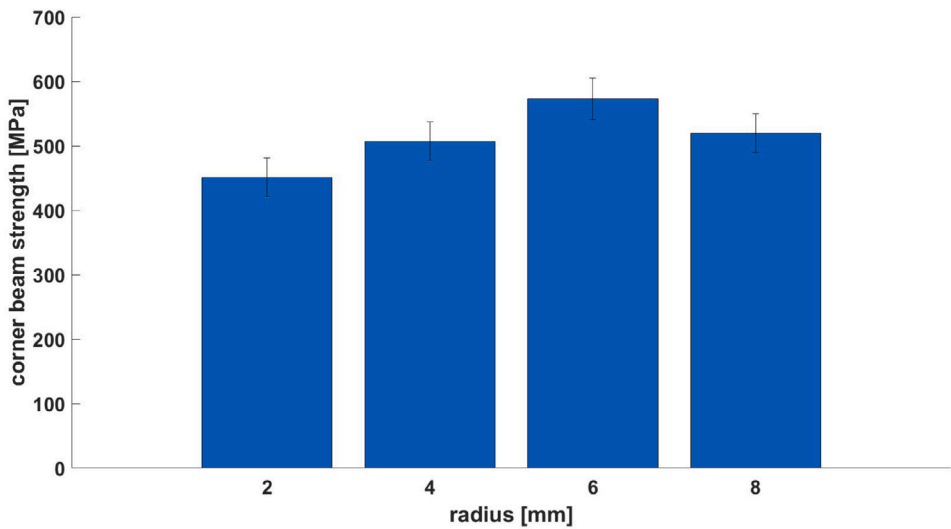**Fig. 13.** Radial strength for different radii (errors bars indicate the standard deviation).

Fig. 14. Corner beam strength for different radii (errors bars indicate the standard deviation).

Table A.3
Overview of the radial stress found for the different manufacturing parameters (standard deviation in brackets).

Box number [–]	Rotational speed [°/s]	Rotational acceleration [°/s^2]	Number of samples tested [–]	Displacement [mm]	Load [N]	CBS [N mm/mm]	Radial strength [MPa]
1	200	1000	8	12.30 (0.38)	595 (41)	235.02 (19.30)	30.80 (2.60)
2	200	1000	4	8.69 (0.14)	1162 (86)	553.99 (32.44)	34.14 (2.48)
3	150	750	4	8.66 (0.72)	1022 (166)	481.04 (56.97)	30.08 (3.90)
4	200	750	8	8.89 (0.45)	1018 (102)	484.09 (34.50)	31.27 (2.27)
5	200	1000	7	9.71 (0.68)	1360 (156)	563.26 (31.69)	30.72 (2.10)
6	150	750	6	10.41 (0.25)	1494 (47)	589.14 (17.88)	32.85 (0.63)
7	100	500	8	10.29 (0.24)	1724 (67)	685.85 (27.03)	36.60 (1.17)

laser power over the complete trajectory, which was not done in the current work since the main focus was to check the quality that can be obtained with the temperature feedback loop implemented.

Interestingly, the data from this test series shows that after delaminations develop, the load carrying capability only drops by about 40%. This damage tolerance is a large advantage for using thermoplastic materials compared to thermoset materials, where the parts often fail catastrophically. The test standard prescribes to stop the test once the load drops below 50% of the maximum load reached during the test, however, this never occurred in the current set of tests.

Finally, the twisting deformation that occurred in some test specimens was caused by the delamination not propagating through the entire width of the sample. This phenomenon indicates that the delamination is arrested within the sample, possibly at the interface between tows, where often a small gap is left to avoid overlaps when the tow width varies. Arresting cracks/delaminations by incorporating small gaps in the structure has been previously shown to be feasible by laser-cutting thin plies into tiles [26], noting that LATP with in-situ consolidation may have this crack-stopping feature inherently. Also the brick-and-mortar structure combined with nanoscale mineral bridges was shown to significantly increase the amount of dissipated energy during fracture [27]. Even though no nanoscale particles are used, the brick-and-mortar structure is used through the thickness of the laminate in the current work, and the small gaps between tracks may act as crack-arrestors. However, this hypothesis is only based on visual observations during the test, and thus needs to be studied in more detail to make a definitive statement on it.

5. Conclusion

In-situ consolidation of thermoplastic structures may be achieved using a combination of winding and laser-assisted tape placement. With this new manufacturing method, the corners become more critical: contrary to traditional manufacturing methods, no L-shaped stiffening elements are present in the corners meaning all the stress is transferred through the composite material. Hence, the corner strength needs to be characterized in more detail. Previously reported results [8] show that the corner strength could be relatively low, but the specimens that were used significantly deviated from the test standard [9] in dimensions, stacking sequence and corner radius.

In the current work, specimens were manufactured and tested according to ASTM Standard D6415 [9]. The rotational speed and acceleration in the corner were varied to determine their influence on the corner strength. Furthermore, a range of different corner radii from 2 to 10 mm were investigated. The tests for specimens with a constant 10 mm radius showed that a lower rotational speed and acceleration lead to a higher radial strength of the corners. When changing the radius, a 2 mm radius, the smallest tested, gave the highest radial

strength. However, the CBS and force at which the first delamination occurs showed a different trend: the changing radius-to-thickness ratio significantly influences the radial strength obtained. The largest force and CBS was obtained for a 6 mm radius, which indicates that at this radius a good compromise between the arc-length of the corner and the decreasing speed before the corner is obtained.

Next to the large radial strength obtained, a load carrying capability of at least 60% of the maximum load was observed after delamination. This relatively high post-damage load-carrying capability was not observed for tests in literature using thermoset material, and is a major advantage of thermoplastic materials. In some tests, the delamination did not propagate through the complete width of the sample, leading to twisting of the samples. The reason for the crack not propagating is not clear, but could be linked to small gaps between tows that remain after manufacturing of the samples.

Overall, the results obtained from this study indicate that the corner strength of carbon fibre-reinforced thermoplastic structures processed by LATP in combination with winding with in-situ consolidation have equivalent or better properties to existing thermoset composite systems and processes. Future work will include examining the effect of increasing the laydown rate to industrially viable levels on corner strength.

CRediT authorship contribution statement

Daniël Peeters: Conceptualization, Methodology, Investigation, Data curation, Formal analysis, Validation, Writing – original draft, Visualization. **David Jones:** Methodology, Investigation. **Ronan O'Higgins:** Conceptualization, Methodology, Visualization, Supervision, Project administration, Resources, Writing – review & editing. **Paul M. Weaver:** Conceptualization, Methodology, Visualization, Supervision, Project administration, Resources, Writing – review & editing, Resources, Funding acquisition.

Declaration of competing interest

The authors declare that they have no known competing financial interests or personal relationships that could have appeared to influence the work reported in this paper.

Data availability

Data will be made available on request.

Table A.4
Overview of the radial stress found for the different radii.

Rotational speed [°/s]	Rotational acceleration [°/s²]	Radius [mm]	Average displacement [mm]	Average force [N]	Average CBS [N mm/mm]	Average radial stress [MPa]
200	1000	2	9.19 (0.38)	1067 (87)	451.24 (30.38)	91.53 (6.45)
200	1000	4	9.72 (0.36)	1236 (95)	507.31 (29.90)	63.39 (3.46)
200	1000	6	9.81 (0.37)	1398 (113)	573.14 (32.27)	51.11 (2.48)
200	1000	8	9.60 (0.34)	1262 (113)	519.94 (30.08)	36.01 (2.02)

Appendix. Test data

See Tables A.3 and A.4.

References

[1] F-22A raptor advanced tactical fighter. 2021, https://www.globalsecurity.org/military/systems/aircraft/f-22-mp.htm (Accessed: 21 April 2021).

[2] Pora J. Composite materials in the airbus A380 - from history to future. In: 13th international conference on composite materials (ICCM19). Beijing, China; 2001.

[3] Comer A, Ray D, Obande W, Jones D, Lyons J, Rosca I, O'Higgins R, McCarthy M. Mechanical characterisation of carbon fibre–PEEK manufactured by laser-assisted automated-tape-placement and autoclave. Composites A 2015;69:10–20.

[4] Stokes-Griffin C, Compston P. The effect of processing temperature and placement rate on the short beam strength of carbon fibre–PEEK manufactured using a laser tape placement process. Composites A 2015;78:274–83.

[5] Qureshi Z, Swait T, Scaife R, El-Dessouky H. In situ consolidation of thermoplastic prepreg tape using automated tape placement technology: Potential and possibilities. Composites B 2014;66:255–67.

[6] Oliveri V, Zucco G, Peeters D, Clancy G, Telford R, Rouhi M, McHale C, O'Higgins R, Young TM, Weaver PM. Design, manufacture and test of an in-situ consolidated thermoplastic variable-stiffness wingbox. AIAA J 2019;1–13.

[7] Bandaru AK, Clancy G, Peeters D, O'Higgins R, Weaver PM. Interface characterization of thermoplastic skin-stiffener composite manufactured using laser-assisted tape placement. In: 2018 AIAA/ASCE/AHS/ASC structures, structural dynamics, and materials conference. 2018.

[8] Peeters D, Clancy G, Oliveri V, O'Higgins R, Jones D, Weaver PM. Concurrent design and manufacture of a thermoplastic composite stiffener. Compos Struct 2019;212:271–80.

[9] ASTM Standard D6415. standard test method for measuring the curved beam strength of a fiber-reinforced polymer-matrix composite. ASTM International; 2002.

[10] Barnes J, Byerly G, LeBouton M, Zahlan N. Dimensional stability effects in thermoplastic composites — towards a predictive capability. Compos Manuf 1991;2(3):171–8, Flow Processes in Composite Materials '91.

[11] Potter K, Khan B, Wisnom M, Bell T, Stevens J. Variability, fibre waviness and misalignment in the determination of the properties of composite materials and structures. Composites A 2008;39(9):1343–54.

[12] çinar K, Ersoy N. Effect of fibre wrinkling to the spring-in behaviour of L-shaped composite materials. Composites A 2015;69:105–14.

[13] O'Connor J. Method for making variable cross section pultruded thermoplastic composite articles. 1989, US Patent 5, 026, 447.

[14] Baran I, Cinar K, Ersoy N, Akkerman R, Hattel JH. A review on the mechanical modeling of composite manufacturing processes. Arch Comput Methods Eng 2017;24(2):365–95.

[15] Lebel LL, Nakai A. Design and manufacturing of an L-shaped thermoplastic composite beam by braid-trusion. Composites A 2012;43(10):1717–29, CompTest 2011.

[16] Lessard H, Lebrun G, Benkaddour A, Pham X-T. Influence of process parameters on the thermostamping of a [0/90]12 carbon/polyether ether ketone laminate. Composites A 2015;70:59–68.

[17] Slange T, Grouve W, Warnet L, Wijskamp S, Akkerman R. Towards the combination of automated lay-up and stamp forming for consolidation of tailored composite components. Composites A 2019.

[18] Peeters D, Jones D, O'Higgins R, Weaver P. Improving the quality of thermoplastic composite corners using laser-assisted tape placement. In: ECCM 2018-18th European conference on composite materials. 2018.

[19] Lekhnitskii SG. Anisotropic plates. Tech. rep., Foreign Technology Div Wright-Patterson Afb Oh; 1968.

[20] Thurnherr C, Groh R, Ermanni P, Weaver P. Investigation of failure initiation in curved composite laminates using a higher-order beam model. Compos Struct 2017;168:143–52.

[21] Charrier J-S, Laurin F, Carrere N, Mahdi S. Determination of the out-of-plane tensile strength using four-point bending tests on laminated L-angle specimens with different stacking sequences and total thicknesses. Composites A 2016;81(Supplement C):243–53.

[22] Avalon SC, Donaldson SL. Strength of composite angle brackets with multiple geometries and nanofiber-enhanced resins. J Compos Mater 2011;45(9):1017–30.

[23] Hao W, Ge D, Ma Y, Yao X, Shi Y. Experimental investigation on deformation and strength of carbon/epoxy laminated curved beams. Polym Test 2012;31(4):520–6.

[24] Wan Y, Goto T, Matsuo T, Takahashi J, Ohsawa I. Investigation about fracture mode and strength in curved section of carbon fiber reinforced polypropylene. In: 19th international conference on composite materials (ICCM19). Montreal, Canada; 2013.

[25] Arca MA, Coker D. Experimental investigation of CNT effect on curved beam strength and interlaminar fracture toughness of CFRP laminates. J Phys Conf Ser 2014;524(1):012038.

[26] Narducci F, Lee K-Y, Pinho S. Realising damage-tolerant nacre-inspired CFRP. J Mech Phys Solids 2018;116:391–402.

[27] Grossman M, Pivovarov D, Bouville F, Dransfeld C, Masania K, Studart AR. Hierarchical toughening of Nacre-like composites. Adv Funct Mater 2019;29(9):1806800.